Heterogeneous Fenton-like oxidation of p-hydroxybenzoic acid using Fe/CeO_2-TiO_2 catalyst

Tijani Hammedi[1,*], Mohamed Triki[2,*], Mayra G. Alvarez[3], Jordi Llorca[4], Abdelhamid Ghorbel[1], Zouhaier Ksibi[1] and Francesc Medina[3]

[1] Université Tunis El Manar, Faculté des Sciences de Tunis, Laboratoire de Chimie des Matériaux et Catalyse, 2092 Tunis, Tunisia

[2] Centre National des Recherches en Sciences des Matériaux, Laboratoire de Valorisation des Matériaux Utiles (LVMU), Pôle Technologique Borj Cedria, 8027 Soliman, Tunisia

[3] Departament d'Enginyeria Química, Universitat Rovira i Virgili, Av/Països Catalans 26, 43007 Tarragona, Spain

[4] Institute of Energy Technologies, Department of Chemical Engineering and Barcelona Research Center in Multiscale Science and Engineering, Universitat Politècnica de Catalunya, EEBE, Eduard Maristany 16, 08019 Barcelona, Spain

*Corresponding authors: E-mails: *tijanihamm@yahoo.fr ; mhtriki@gmail.com*

Word count: 5435

ABSTRACT

This paper is built on the Fenton-like oxidation of p-hydroxybenzoic acid (p–HBZ) in the presence of H_2O_2 and 3%Fe supported on CeO_2-TiO_2 aerogels under mild conditions. These catalysts were deeply characterized by XRD, H_2-TPR, TEM, STEM and XPS. The effect of thermal treatment, pH (2-3, 5, 7), H_2O_2/p–HBZ molar ratio (5, 15, 20, 25) and reaction temperature (25 °C, 40 °C and 60 °C) on the catalytic properties of supported Fe catalysts are studied. Our results highlight the role of CeO_2 and the calcination of the catalyst to obtain the highest catalytic properties after 10 min: 73% of p–HBZ conversion and 52% of TOC abatement.

Key words Fenton-like oxidation, p-hydroxybenzoic acid, Fe catalyst, CeO_2

INTRODUCTION

Advanced oxidation processes (AOPs) have been successfully used for the treatment of wastewaters to reduce the concentration of toxic organic pollutants. This technology is based on the *in situ* generation of hydroxyl radicals ($HO^{\bullet}$), which are highly reactive and non-selective. Wet hydrogen peroxide oxidation is one of the AOPs technologies, which is known to be efficient for the degradation of organic pollutants using hydrogen peroxide as the liquid oxidant (Hu & Long 2016; Kurian & Nair 2015). Since this process requires severe operation conditions and costing investment, many efforts have been made to use it at milder conditions by an appropriate catalyst (Rokhina & Virkutyte 2011). In this context, heterogeneous Fenton-like reaction based on nanomaterials at mild conditions has gained attention as one of the most important catalytic processes for the oxidation of dissolved organic pollutants (Bokare & Choi 2014; Hartmann *et al.* 2010; Munoz *et al.* 2015; Pouran *et al.* 2014). Recently, several heterogeneous catalysts have been studied in Fenton like oxidation of different organic contaminants such as Magnetite/Fe-Al-montmorillonite (Wei *et al.* 2017), CuFe-carbon (Wang *et al.* 2015), Iron-alumina (Di Luca *et al.* 2015), Ag/CeO_2 (Aneggi *et al.* 2017) and CeO_2–H_2O_2 system with Fe^{3+} doping (Cai *et al.* 2010). Moreover, CeO_2 is able to activate H_2O_2 by a Fenton-like reaction due to the availability of Ce^{3+} oxygen vacancies on the oxide surface (Mamontov *et al.* 2000). In addition to that, the oxidation-reduction process of the Ce species occurs more easily on the surface of the particle (Ce^{4+}/Ce^{3+}, cycle), producing an easy formation and elimination of oxygen defects during catalytic applications (Campbell & Peden 2005). The use of CeO_2 as heterogeneous Fenton-like catalyst by generating $HO^{\bullet}$ radicals was proved in the presence of H_2O_2 (Heckert *et al.* 2008) as shown by the following reactions:

$$Ce^{3+} + H_2O_2 + H^+ \rightarrow Ce^{4+} + HO^{\bullet} + H_2O \quad (1)$$

$$HO^{\bullet} + H_2O_2 \rightarrow HO_2^{\bullet} + H_2O \quad (2)$$

$$Ce^{4+} + HO_2^{\bullet} \rightarrow Ce^{3+} + O_2 + H^+ \quad (3)$$

As mentioned in previous studies, the $HO^{\bullet}$ production depends critically on the oxide surface properties (Ji *et al.* 2010). Without surface modification, the reaction between Ce^{3+} and H_2O_2 leads to the formation of stable brown peroxide-like species ($Ce^{3+}-OOH^-$), which remain stable even at neutral pH and do not directly decompose to generate free $HO^{\bullet}$ (Chen *et al.* 2012). The peroxide species are relatively chemically stable in the absence of organic contaminants and can only degrade substances absorbed on the surface of CeO_2 via an intermolecular rearrangement. As shown in schema (1), the degradation of organics is a localized surface reaction rather than a radical-attack Fenton reaction in the CeO_2/H_2O_2 system (Wang *et al.* 2014).

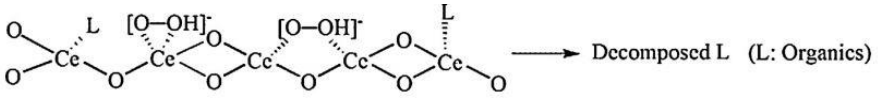

Schema (1)

Thus, the heterogeneous redox system CeO_2-H_2O_2 can be easily manipulated by simple surface modification to efficiently generate $HO^{\bullet}$ under mild acidic condition. The use of CeO_2 further amplifies the effective surface concentration of Ce^{3+} and increases the overall $HO^{\bullet}$ yield, due to the critical role of surface Ce^{3+} species on the catalytic efficiency. In our previous work, we found that CeO_2, when associated with TiO_2, promotes oxygen storage and enhances oxygen mobility, producing surface and bulk vacancies that improve the redox properties of the catalytic system (Hammedi *et al.* 2015a). However, the CeO_2-TiO_2 mixed oxides have not been investigated yet as supports for catalysts in Fenton-like oxidation.

In this work, we explored the efficiency of the 3%Fe/CeO_2-TiO_2 catalysts for the Fenton-like oxidation of p-hydroxybenzoic acid (p–HBZ) in the presence of H_2O_2 at mild conditions. This molecule was chosen as a non-biodegradable model of phenolic pollutants typically found in olive oil mill wastewaters. We thoroughly studied the effect of pH, H_2O_2 concentration and

reaction temperature on the catalytic properties of supported Fe catalysts. The CeO_2-TiO_2 mixed oxides as well as the Fe catalysts were deeply characterized by XRD, H_2-TPR, TEM, STEM and XPS.

EXPERIMENTAL

Catalysts preparation

CeTi and TiO_2 were prepared via the sol-gel method as described previously (Hammedi *et al.* 2015a). CeTi was prepared by dissolving Cerium(III) nitrate hexahydrate in anhydrous ethanol in the presence of ethyl acetoacetate. Titanium(IV) isopropoxide was then added to the mixture in different molar ratios of Ce/Ti: 1/4, 1/5 and 1/6. Homogeneous gels, obtained after addition of HNO_3 (0.1 mol/L), were transferred to an autoclave for a supercritical drying at T=243 °C and P=64 bars. All samples were calcined under oxygen at 500 °C for 3 h. TiO_2 was prepared by the same described protocol without the addition of the cerium salt. The Fe (3 wt%) catalysts were prepared by incipient wetness impregnation of the support with an aqueous solution of $Fe(NO_3)_3.9H_2O$. The obtained solids were dried overnight at 90 °C for 24 h and then calcined under O_2 at 300 °C for 2 h. The samples were named as 3Fe/Ti–C and 3Fe/CeTi–C. Some samples were reduced under H_2 for 2 h at 300 °C and labelled as 3Fe/CeTi–R.

Catalysts characterization

N_2 physisorption studies were carried out in automatic Micromeritics ASAP 2020 apparatus. The specific surface area was determined using the Brunauer-Emmett-Teller (BET) method and the average pore size was calculated with the Barrett-Joyner-Halenda (BJH) method using isothermal desorption data. X-ray diffraction (XRD) measurements were performed using a Philips PW1050 diffractometer. The average crystallite size of the samples was estimated using the Debye-Scherrer equation. Hydrogen temperature programmed reduction (H_2-TPR) profiles were obtained on a Micromeritics Autochem 2920 analyzer TPD/R/O using a thermal

conductivity detector. The catalyst was treated under O_2(5%)/He at 300 °C for 1 h and then reduced from 40 °C to 700 °C with H_2(5%)/Ar (30 mL/min). Transmission electron microscopy (TEM) images were acquired using a JEOL JEM-1011 microscope operating at 80 kV. High-angle annular dark-field scanning transmission electron microscopy (STEM) and energy dispersive X-ray analysis (EDX) were carried out at 200 kV with a Tecnai G2 F20 S-TWIN instrument equipped with a field emission electron source. X-ray photoelectron spectroscopy (XPS) was performed on a SPECS system equipped with an Al anode XR50 source operating at 150 mW and a Phoibos MCD-9 detector. The pass energy of the hemispherical analyzer was set at 25 eV and the energy step was set at 0.1 eV. The pressure in the analysis chamber was kept below 10^{-7} Pa.

Catalytic oxidation experiments

Catalytic tests were performed in a glass reactor at atmospheric pressure using 100 mL of p–HBZ aqueous solution (10 mmol/L) over supported Fe catalyst (30 mg) at fixed pH and temperature between 25 °C and 60 °C. The desired pH (2, 3.2, 5 and 7) of the solution was adjusted using HCl (0.1 mmol/L) or NaOH (0.1 mmol/L). After stirring for 30 min in order to reach the p–HBZ adsorption equilibrium, a volume of H_2O_2 was added to the solution and the reaction started. It is important to note that samples were withdrawn to assess adsorption before the addition of H_2O_2. The H_2O_2/p–HBZ molar ratio of 14/1 corresponds to the stoichiometric quantity needed for the total oxidation of p–HBZ to CO_2 and H_2O according to the following reaction:

$$C_7H_6O_3 + 14H_2O_2 \rightarrow 7CO_2 + 17H_2O \quad (4)$$

Therefore, 0.123 mL of H_2O_2 (11 mol/L) was added into the reactor to get a H_2O_2/p–HBZ molar ratio of 14/1. Different H_2O_2/p–HBZ molar ratios (5, 15, 20 and 25) are studied. The concentrations of p–HBZ and intermediates were monitored by high performance liquid chromatography (HPLC, Waters 1515) at λ=254 nm using a Hypersil Gold C18 column and

acetonitrile/H_2O/H_2SO_4 (0.005 mol/L) (20/70/10) as mobile phase. Total Organic Carbon (TOC) was measured with a Shimadzu Model 5050 TOC analyzer. The initial reaction rate was calculated from the curve C *versus* time where C is the concentration of p–HBZ after oxidation. It corresponds to the slope of the linear part of the curve at low p–HBZ conversion (< 10% of conversion).

RESULTS AND DISCUSSION

Catalysts characterization

Table 1 shows the textural and structural properties of the prepared materials. BET surface areas of the CeO_2-TiO_2 materials are higher than the area obtained for pure TiO_2. This result could be attributed to the inhibition of particles growth for the CeTi mixed oxides, which can be verified by TEM analysis. As the content of cerium increases, the S_{BET} of CeTi increases to 183 m^2/g for a Ce/Ti ratio of 1/5. This result could be due to the modification of the hydrolysis-condensation reactions rates by the cerium nitrate (Lopez *et al.* 2004). However, a decrease in pore diameter is observed when adding Ce to TiO_2, which could be due to the higher bond length of Ce–O (2.343 Å) (Shoko *et al.* 2009) compared to the bond length of Ti–O (1.952 Å) (Brown & Shannon 1973). BET surface areas of the supported Fe catalysts are lower than those of bare CeTi. In fact, the S_{BET} of 3Fe/CeTi–C and 3Fe/CeTi–R are 133 m^2/g and 142 m^2/g, respectively compared to 183 m^2/g for the CeTi(1/5) support. This result could be attributed to a certain blockage of the porous structure of the support by Fe species.

Materials	S_{BET} (m^2/g)	Pore diameter (nm)	TiO_2 crystallite size[a] (nm)
TiO_2	82	21.0	49
CeTi(1/4)	110	19.7	40
CeTi(1/5)	183	9.0	9.0
CeTi(1/6)	124	16.7	10
3Fe/Ti–C	76	8.8	83
3Fe/CeTi–C	133	11.4	40
3Fe/CeTi–R	142	10.7	24

[a]By XRD.

Figure 1 shows the XRD patterns of TiO_2, CeTi, 3Fe/Ti–C and 3Fe/CeTi. For TiO_2, only peaks corresponding to anatase phase were detected (JCPDS 83-2243). For CeO_2, peaks at 2θ=28.6°, 33.1°, 47.5° and 56.3° attributed to cubic structure were observed (JCPDS 43-1002). For the CeTi mixed oxides, peaks corresponding to TiO_2 anatase become weaker and broader, while peaks corresponding to CeO_2 are weaker, compared to those of pure oxides. Moreover, the crystallite size of TiO_2 in CeTi decreases, which suggests that the Ce species inhibit the growth of anatase crystallites (Table 1). The appearance of CeO_2 phase simultaneously with the decrease of TiO_2 particle size is consistent with BET surface area results. The XRD patterns of Fe/CeTi are similar to those of CeTi without any crystalline phase corresponding to iron oxide. It can be noticed that TiO_2 crystalline phase in the 3Fe/CeTi–R catalyst is lower than in the calcined one (3Fe/CeTi–C). This result indicates that the reduction of the catalyst could lead to the segregation of iron particles in the CeTi mixed oxides.

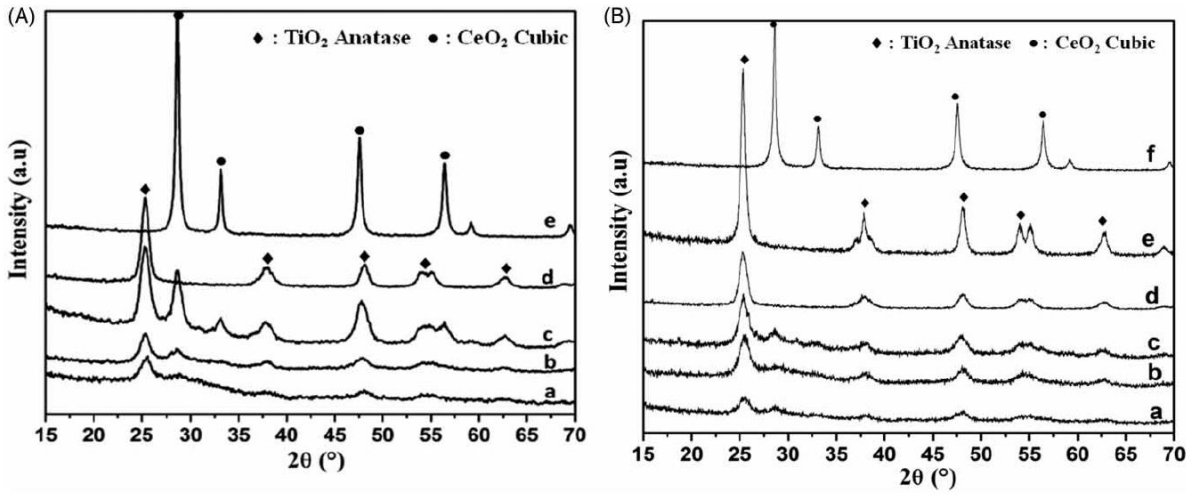

Figure 2 shows the H_2–TPR profiles of the samples. Pure CeO_2 (Figure 2(a)) exhibits a broad reduction peak at 530 °C, which could be attributed to the reduction of Ce^{4+} to Ce^{3+} on the surface (Dutta *et al.* 2006). For the CeTi support (Figure 2(b)), the H_2–TPR profile exhibits a broad reduction peak between 250 °C and 500 ºC (maximum at 460 ºC), which is shifted to lower reduction temperatures compared to pure ceria. Therefore, the reduction of CeO_2 in the mixed support is facilitated in comparison with pure CeO_2. A broad peak for 3Fe/CeTi–C (Figure 2(c)) is observed at 330 ºC, probably due to the reduction of iron oxide in strong interaction with the support (Hammedi *et al.* 2015b). For 3Fe/CeTi–R, a reduction peak is observed at 305 ºC (Figure 2(d)), where the amount of hydrogen consumed (607 µmol/g) is similar to that of the calcined sample (585 µmol/g), which suggests that during the reduction the iron oxide species strongly interact with the CeTi support. For the 3Fe/Ti–C sample (Figure 2e), two broad reduction peaks are observed at 150 and 650 ºC. The first peak is due to the presence of iron with no interaction with the TiO_2 support, while the second peak is probably due to the iron in the crystalline structure of the TiO_2 support.

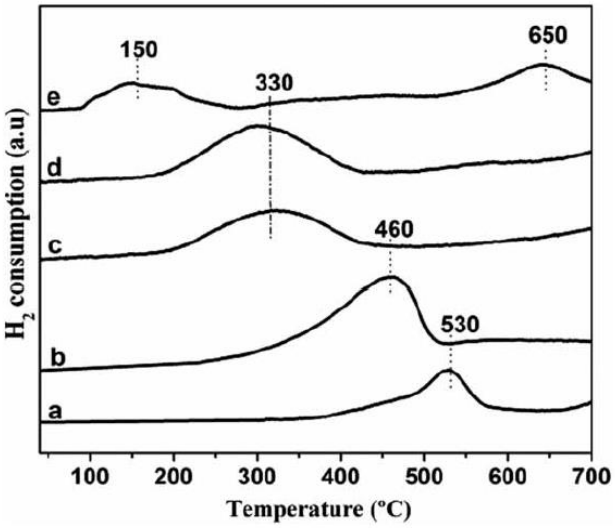

Figure 3 presents TEM images of TiO_2, CeTi, 3Fe/CeTi–R and 3Fe/CeTi–C. Slight aggregates of TiO_2 particles are observed (Figure 3(a)), although better dispersion is achieved by doping with CeO_2 (Figure 3(b)). This observation could explain the fact that the BET surface area of CeTi is higher than the area obtained for pure TiO_2. Since the Fe–Ce ions are inserted into the lattice of TiO_2, the particles in 3Fe/CeTi–C (Figure 3(c)) and 3Fe/CeTi–R (Figure 3(d)) are well dispersed. STEM images of 3Fe/CeTi-C show well-dispersed iron particles at high magnification with no large aggregates *(Figure S1, Supplementary information*). EDX analysis (*Inset in Figure S1a)* shows a uniform distribution of iron particles of 1-2 nm.

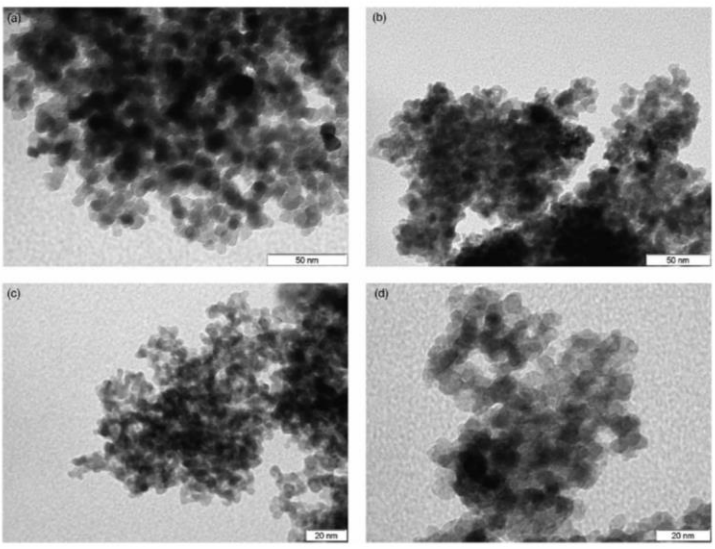

XPS spectra of 3Fe/CeTi-C are shown in Figure 4 and the surface atomic ratios Ce/Ti, Fe/Ti and Fe/(Ce+Ti) are given in *Table S1 (Supplementary information)*. The surface atomic Ce/Ti decreased in the presence of the iron species, which shows that Ce probably interacts with Fe particles. The XPS spectrum of the Fe2p region taken on the surface of 3Fe/CeTi-C (Figure 4(a)) shows the presence of satellite lines, indicating the presence of oxidized Fe (Nasralla *et al.* 2013). The XPS spectrum of Ce3d for 3Fe/CeTi–C (Figure 4(b)) reveals the presence of both Ce(III) and Ce(IV). The CeTi sample contained 17.2% of reduced Ce(III), whereas 3Fe/CeTi-C contained 22.2% of Ce(III). This means that the transition metal promotes the reduction of CeO_2 on the surface, suggesting a strong contact between the metal nanoparticles and the support. Ce^{3+} induces the formation of oxygen vacancies in the material, which are essential for adsorption/dissociation of oxygen molecules during the oxidation. The XPS spectrum of Ti2p for 3Fe/CeTi–C (Figure 4(c)) indicates the presence of Ti^{4+} in the CeTi mixed oxides. The XPS binding energy of O1s at 530.4 eV is assigned to lattice oxygen, while the peak at 532.8 eV is ascribed to surface hydroxyl species (Figure 4(d)).

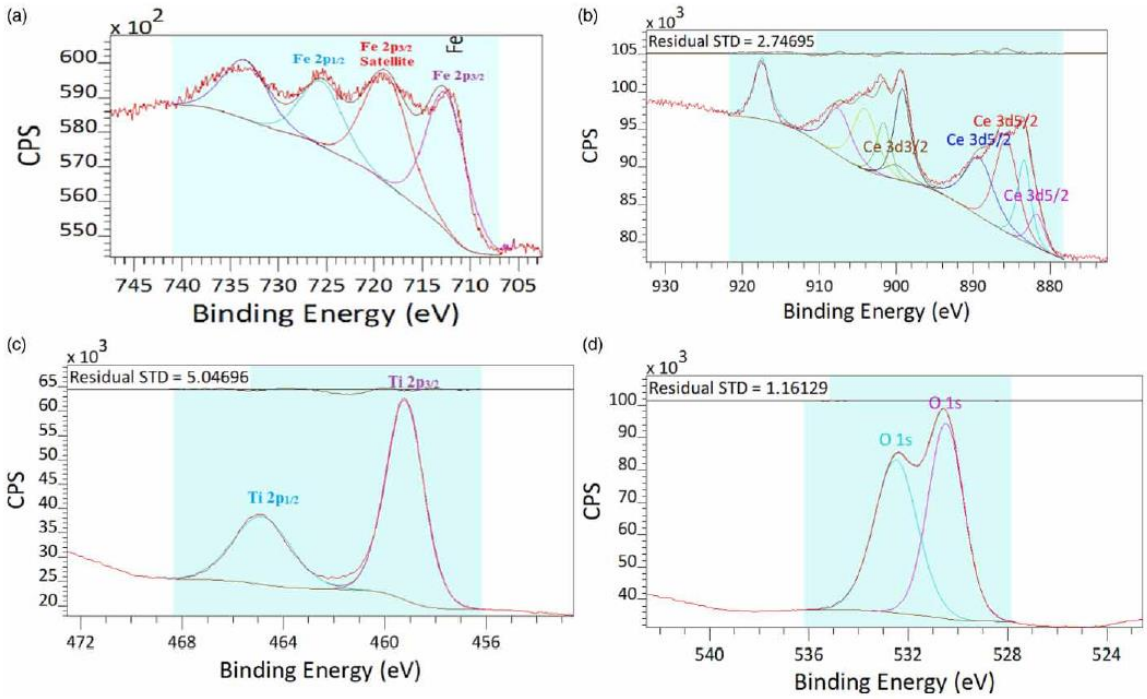

Catalytic results

Blank experiments were carried out to evaluate the eventual contribution of the non-catalytic system in p–HBZ oxidation and H_2O_2 decomposition. The results show that, without catalyst, the oxidation of p–HBZ and the decomposition of H_2O_2 are negligible at 60 °C using a (H_2O_2/p–HBZ) molar ratio of 14/1. Moreover, the results show that the adsorption of p–HBZ on the solid remains below 5.0%. In order to fix the amount of catalyst, experiments were performed in the presence of 3Fe/CeTi–C (15 mg, 20 mg and 30 mg) at 60 °C. We chose to perform the reaction with 30 mg of catalyst to ensure that there are no mass transfer limitations as shown in *Figure S2 (Supplementary information)*. Table 2 regroups the initial reaction rates and the catalytic properties of supported Fe catalysts for the oxidation of p–HBZ at 60 °C. The results show that 3Fe/CeTi–C leads to 73% of p–HBZ conversion after 10 min, compared to 37% with 3Fe/Ti–C and 2.5% with 3Fe/CeTi–R. These results could be related to the fact that 3Fe/CeTi-C presents a high surface area, high content of oxygen vacancies and a high concentration of Ce^{3+}, permitting enhancement of oxygen adsorption on the catalyst surface, and so increasing the catalytic activity. In addition, the initial reaction rates of the supported Fe catalysts are quite high. However, the calcined catalyst (3Fe/CeTi–C) is more active than 3Fe/CeTi–R since its initial reaction rate reaches 0.166 mmol/(g•min) compared to 0.11 mmol/(g•min) for the reduced catalyst. The low initial reaction rate showed by the reduced catalyst suggests an induction period needed for this catalyst (3Fe/CeTi–R). This period could be due to a reduced concentration of chemisorbed oxygen and/or weakly bonded oxygen species on the CeTi mixed oxides. Despite 3Fe/CeTi–C and 3Fe/CeTi–R show similar TPR profiles, it seems reasonable that the reduction step provokes changes at the material surface, which is mirrored on the catalytic activity. This reduction removes the surface oxygen species, so a re-oxidation step is necessary before the Fenton reaction. Hydroquinone and maleic acid are identified as intermediates and the evolution of their

concentrations during the oxidation of p–HBZ over 3Fe/Ti–C, 3Fe/CeTi–C and 3Fe/CeTi–R is shown in Figure 5. Hydroquinone is produced at higher concentration, while maleic acid is produced at a lower concentration. In the presence of 3Fe/Ti–C, the concentration of hydroquinone reaches 0.397 mmol/L after 10 min and then decreases slightly after 1 h of reaction. However, the 3Fe/CeTi–C catalyst leads to the highest hydroquinone concentration (0.478 mmol/L) after 10 min, which decreases rapidly after 30 min of reaction.

				Selectivity (%) at 10 min	
Catalysts	**R_0[a] (mmol/(g•min))**	**TOC abatement (%) after 1 h**	**p–HBZ conversion (%) after 10 min**	**Hydroquinone**	**Maleic acid**
3Fe/Ti–C	0.150	48	37	5.9	0.03
3Fe/CeTi–C	0.166	52	73	15.0	0.31
3Fe/CeTi–R	0.110	42	2.5	1.2	0.06

[a]Initial reaction rate.

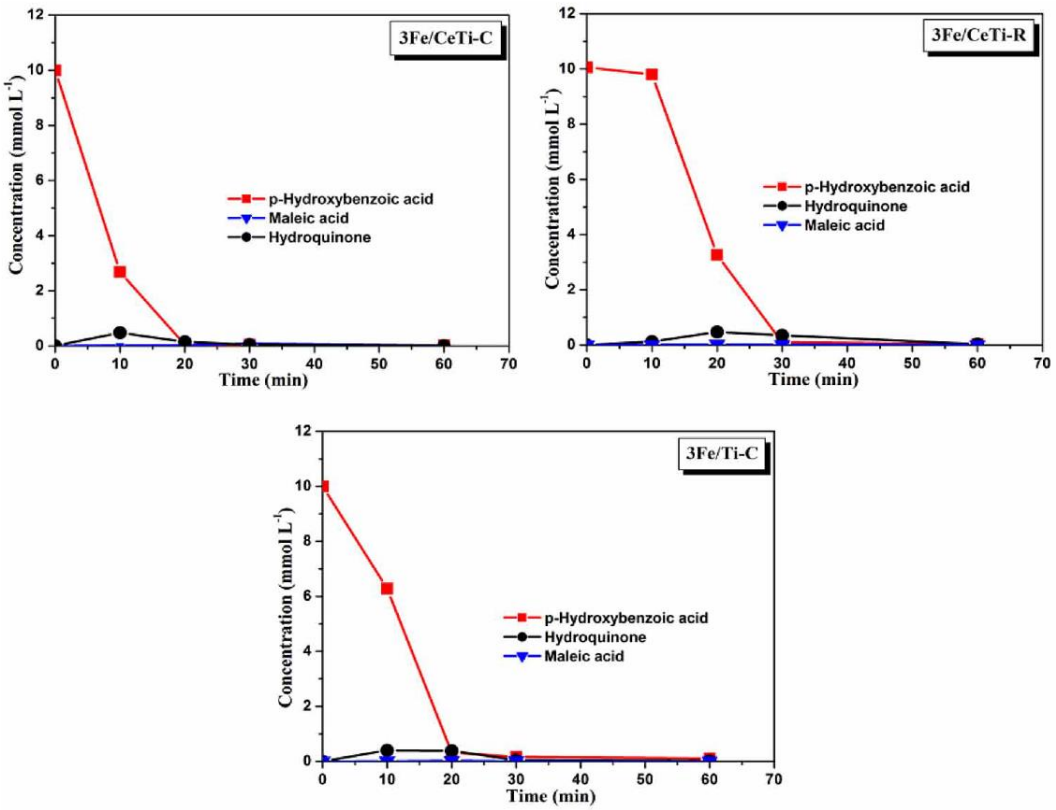

Effect of pH

The effect of pH on p–HBZ oxidation over 3Fe/CeTi–C in the presence of H_2O_2 is shown in Figure 6. The results show that the catalytic properties are affected when pH increases. In fact, p–HBZ conversion is higher than 70% after 10 min at pH 2–3, whereas it decreases to

12% and 1.0% at pH 5 and pH 7, respectively. This result could be related to a decrease of the oxidation potential of •OH due to the increase of pH (Kwnon *et al.* 1999). Moreover, some active iron species cannot exist at neutral pH and thus cannot establish an effective Fenton-like reaction. When pH decreases, a sufficient amount of H_2O_2 is available producing hydroxyl radicals due to the generation of carboxylic acids. However, when pH increases, precipitation of insoluble ferric hydroxides takes place and the decomposition of H_2O_2 becomes preponderant. Therefore, at high pH, hydrogen peroxide is decomposed into H_2O and O_2 due to the iron precipitate, which suppresses the •OH generation. Due to this decomposition, fewer hydroxyl radicals are formed and so weaker degradation efficiency is achieved (Sreeja & Sosamony 2016). It could be concluded that pH value affects the formation of •OH radicals and so the degradation efficiency, which reaches the maximum at pH 2, in the photo-Fenton-like processes. In our previous work (Hammedi *et al.* 2015b), no Fe leaching with high extent was observed and the inductive coupled plasma analyses showed that the maximum of Fe concentration detected in the solution was 5.4 mg/L at pH 3.4 after 1 h of reaction. This represents a leaching of 6.0% of Fe in the solution, indicating reasonably good stability in acidic pH, and probably the amount of leached Fe at higher pH could be considered negligible. A small contribution due to homogeneous Fenton might occur. However, this amount of leached Fe do not probably have a great effect on the p–HBZ oxidation rate, since it was found that the catalytic activity is related to Fe concentrations of 10 times higher than those found in our solutions (Rivas *et al.* 2001). Moreover, it is important to take into account that Fe leaching has to be produced progressively, thus a low amount of Fe could be found at the first minutes of reaction. For this reason, a heterogeneous mechanism of p–HBZ is most probably expected to occur. On the other hand, CeO_2 seems to improve the catalytic stability by strengthening the interaction between Fe and the CeTi mixed oxides as found by H_2-TPR, which may lead to low Fe leaching.

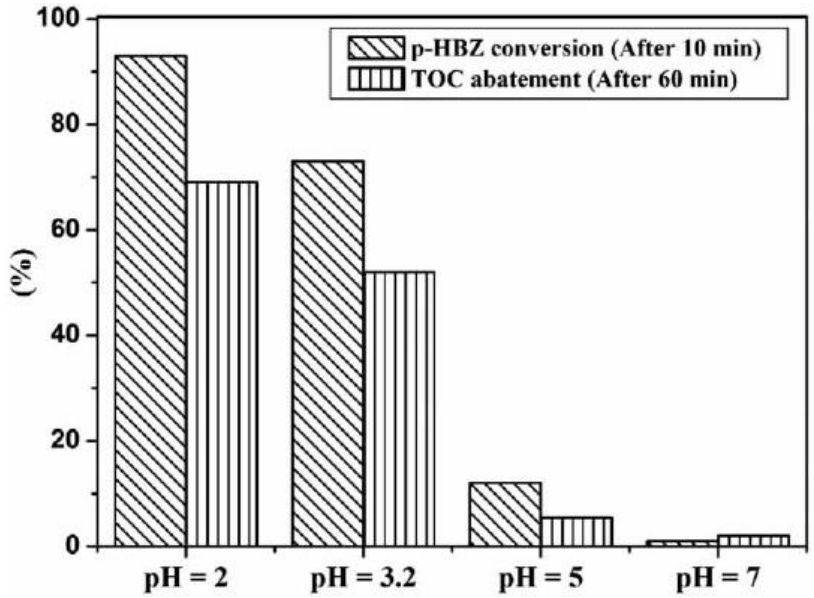

Effect of H_2O_2/p–HBZ molar ratio

The Fenton-like oxidation of p–HBZ carried out by •OH, produced directly from the reaction between H_2O_2 and Fe catalyst supported on CeTi. The choice of optimal H_2O_2/p–HBZ molar ratio, permitting the highest oxidation efficiency, is important from a practical point of view due to the cost of H_2O_2. Figure 7 shows the effect of H_2O_2 concentration on p–HBZ conversion and TOC abatement when p–HBZ oxidation was performed over 3Fe/CeTi–C at 60 °C. It can be noted that the conversion of p-HBZ is enhanced with the increase of the H_2O_2/p–HBZ molar ratio. A total conversion of p–HBZ is achieved after 20 min for H_2O_2/p–HBZ molar ratios of 15 and 20. This result could be attributed to the presence of more •OH radicals on the surface of 3Fe/CeTi–C, which is in accordance with previous studies (Chang *et al.* 2018). However, when the H_2O_2/p–HBZ molar ratio is 25, the degradation efficiency is decreased to 78%. Therefore, the further increase in H_2O_2 concentration does not lead to higher oxidation rate, which could probably be due to a scavenging effect of •OH. In fact, •OH is a powerful scavenger, which may react with H_2O_2 according to the following reactions:

$$H_2O_2 + {}^{\bullet}OH \rightarrow HO_2^{\bullet} + H_2O \quad (5)$$

$$HO_2^{\bullet} + {}^{\bullet}OH \rightarrow O_2 + H_2O \quad (6)$$

The hydroperoxyl radical ($HO_2^{\bullet}$) generated is less reactive than $^{\bullet}OH$ and does not contribute to the degradation of organic pollutants, which only occurs in the presence of $^{\bullet}OH$ radical (Shukla *et al.* 2010; Liu *et al*. 2017). Therefore, an appropriate molar ratio of H_2O_2/p–HBZ is required to avoid the excess of H_2O_2 and so the decrease of degradation efficiency.

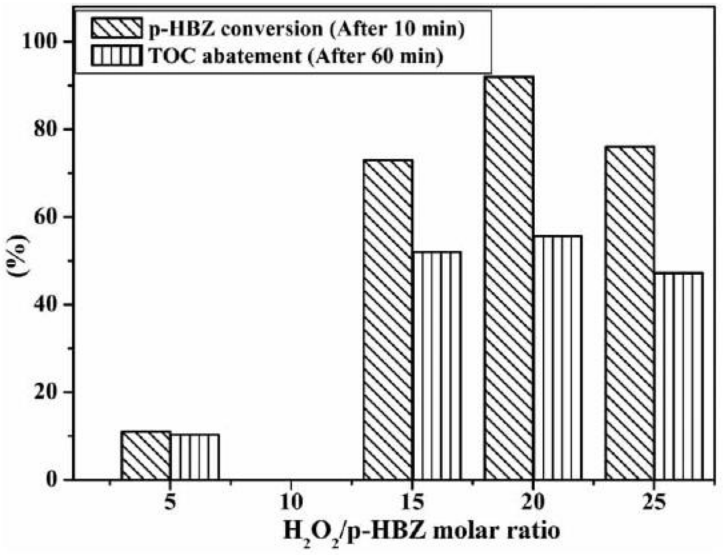

Effect of reaction temperature

The effect of reaction temperature on the catalytic behavior of 3Fe/CeTi–C is shown in Table 3. As expected, p–HBZ conversion and TOC abatement are enhanced when the temperature increases. In fact, p–HBZ conversion increases from 7.0% to 25% at 25 °C and 40 °C, respectively, and reaches 73% at 60 °C after 10 min of reaction. Moreover, the initial reaction rates increase from 0.02 mmol/(g·min) at 25 °C to 0.166 mmol/(g·min) at 60 °C. This result could be due to a higher rate of H_2O_2 conversion into $^{\bullet}OH$ at higher temperature leading to a smaller amount of H_2O_2 to scavenge these radicals (Inchaurrondo *et al.* 2012).

	25 °C	40 °C	60 °C
R_0^a (mmol/(g•min))	0.020	0.081	0.166
p–HBZ conversion (%) after 10 min	7.0	25	73
TOC abatement (%) after 1 h	37	48	52

[a]Initial reaction rate.

Kinetic study

To reveal the catalytic reaction kinetics, $\ln(C_0/C_t)$ *versus* time at different temperatures are plotted as shown in Figure 8. The linear fit of $\ln(C_0/C_t)$ *versus* time indicates that the oxidation of p–HBZ follows a pseudo-first order kinetic. Therefore, the following equation can be applied:

$$\ln(C_0/C_t) = (k_{app}).t \quad (7)$$

where C_0 and C_t are the concentrations of p–HBZ (mmol/L) at time 0 (min) and t (min), respectively, and k_{app} is the apparent reaction rate constant (min^{-1}).

It is obvious that the apparent reaction rate constant is improved with increasing the reaction temperature. Accordingly, the apparent reaction rate constants are 0.007 min^{-1}, 0.029 min^{-1} and 0.125 min^{-1} at 25 °C, 40 °C and 60 °C, respectively. In fact, p–HBZ oxidation is faster at high temperature due to rapid activation of H_2O_2. It is important to note that the temperature should be below 80 °C to prevent the decomposition of H_2O_2 into O_2 and H_2O. The activation energy (E_a) could be calculated according to the following Arrhenius equation:

$$\ln k_{app} = \ln A - E_a/RT \quad (8)$$

where A is the Arrhenius factor and k_{app} is the apparent reaction rate constant (min^{-1}).

The activation energy can be calculated from the slope of the $\ln k_{app}$ *versus* 1/T linear curve (*Figure S3, supplementary information*). The E_a value is determined as 67.8±0.5 kJ/mol for the p–HBZ oxidation over 3Fe/CeTi–C.

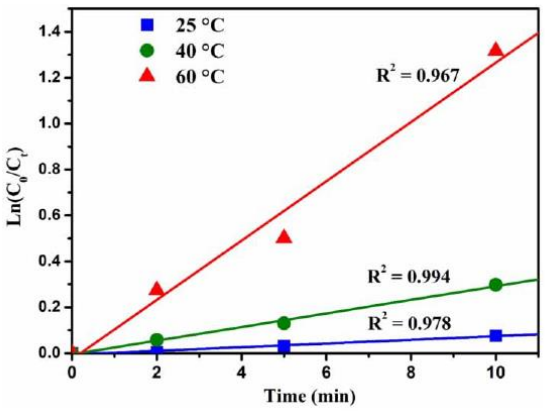

CONCLUSIONS

3%Fe supported on CeO_2-TiO_2 aerogels are prepared, characterized and evaluated in the oxidation of p–HBZ in the presence of H_2O_2 at mild conditions. This oxidation could be considered as a Fenton-like reaction due to the production of $HO^{\bullet}$ from H_2O_2 and Fe supported catalyst. 3Fe/CeTi–C shows the best catalytic properties, at conditions of pH 3.2, 60 °C and H_2O_2/p–HBZ molar ratio of 14, compared to the reduced one. This catalyst reaches 0.166 mmol/(g•min) of initial reaction rate, 73% of p–HBZ conversion after 10 min and 52% of TOC abatement after 1 h. CeO_2 plays an important role in these good catalytic properties; this closely relies on the synergistic effect with TiO_2 allowing better O_2 availability to active sites due to the redox cycle of Ce^{4+}/Ce^{3+}. Further studies are required to characterize the catalyst after reaction and to check the catalyst stability in a continuous reactor. One important direction for our future work would be a greater focus on the Fenton-like oxidation of real wastewaters using supported Fe catalysts.

ACKNOWLEDGMENTS

Tunisian Ministry of Higher Education and Scientific Research and Spanish Ministry of Economy and Competitiveness are acknowledged for their financial support. F. Medina and J. Llorca would like to thank the Generalitat de Catalunya for the ICREA Academia Award.

REFERENCES

Aneggi, E., Trovarelli, A. & Goi, D. 2017 Degradation of phenol in wastewaters via heterogeneous Fenton-like Ag/CeO_2 catalyst. *Journal of Environmental Chemical Engineering* **5**, 1159-1165.

Brown, I. D. & Shannon R. D. 1973 Empirical bond- strength–bond- length curves for oxides, *Acta Crystallographica A* **29**, 266-282.

Bokare, A. D. & Choi, W. 2014 Review of iron-free Fenton-like systems for activating H_2O_2 in advanced oxidation processes. *Journal of Hazardous Materials* **275**, 121-135.

Cai, W., Chen, F., Shen, X., Chen, L. & Zhang, J. 2010 Enhanced catalytic degradation of AO7 in the CeO_2–H_2O_2 system with Fe^{3+} doping. *Applied Catalysis B* **101**, 160-168.

Campbell, C. T. & Peden, C. H. 2005 Oxygen Vacancies and Catalysis on Ceria Surfaces. Science **309**, 713-714.

Chang, F., Wu, F., Zheng, J., Cheng, W., Yan, W., Deng, B. & Hu, X. 2018 *In-situ* establishment of binary composites α-Fe_2O_3/$Bi_{12}O_{17}Cl_2$ with both photocatalytic and photo-Fenton features. *Chemosphere* **210**, 257-266.

Chen, F., Shen, X., Wang, Y. & Zhang, J. 2012 CeO_2/H_2O_2 system catalytic oxidation mechanism study via a kinetics investigation to the degradation of acid orange 7. *Applied Catalysis B* **121-122**, 223-229.

Di Luca, C., Ivorra, F., Massa, P. & Fenoglio, R. 2015 Iron-alumina synergy in the heterogeneous Fenton-type peroxidation of phenol solutions. *Chemical Engineering Journal* **268**, 280-289.

Dutta, G., Waghmare, U. V., Baidya, T., Hegde, M. S., Priolkar, K. R. & Sarode, P. R. 2006 Origin of Enhanced Reducibility/Oxygen Storage Capacity of $Ce_{1-x}Ti_xO_2$ Compared to CeO_2 or TiO_2. *Chemical Materials* **18**, 3249-3256.

Guo, L., Chen, F., Fan, X., Cai, W. & Zhang, J. 2010 S-doped α-Fe_2O_3 as a highly active heterogeneous Fenton-like catalyst towards the degradation of acid orange 7 and phenol. *Applied Catalysis B* **96**, 162-168.

Hammedi, T., Triki, M., Ksibi, Z., Ghorbel, A. & Medina, F. 2015a Comparative study of textural, structural and catalytic properties of xerogels and aerogels CeO_2–TiO_2 mixed oxides. *Journal of Porous Materials* **22**, 939-948.

Hammedi, T., Triki, M., Ksibi, Z., Ghorbel, A. & Medina, F. 2015b Catalytic wet hydrogen peroxide oxidation of p-hydroxybenzoic acid over Fe/TiO_2 and 0.5Ru–3Fe/TiO_2. *Journal of Sol Gel Science and Technology* **76**, 679-685.

Hartmann, M., Kullmann, S. & Keller, H. 2010 Wastewater treatment with heterogeneous Fenton-type catalysts based on porous materials. *Journal of Materials Chemistry* **20**, 9002-9017.

Heckert, E. G., Seal, S. & Self, W. T. 2008 Fenton-Like Reaction Catalyzed by the Rare Earth Inner Transition Metal Cerium. *Environmental Science and Technology* **42**, 5014-5019.

Hu, P. & Long, M. 2016 Cobalt-catalyzed sulfate radical-based advanced oxidation: A review on heterogeneous catalysts and applications. *Applied Catalysis B* **181**, 103-117.

Inchaurrondo, N. S., Massa, P., Fenoglio, R., Font, J. & Haure, P. 2012 Efficient catalytic wet peroxide oxidation of phenol at moderate temperature using a high-load supported copper catalyst. *Chemical Engineering Journal* **198-199**, 426-434.

Ji, P., Wang, L., Chen, F. & Zhang, J. 2010 Ce^{3+}-Centric Organic Pollutant Elimination by CeO_2 in the Presence of H_2O_2. *ChemCatChem* **2**, 1552-1554.

Kurian, M. & Nair, D. S. 2015 Heterogeneous Fenton behavior of nano nickel zinc ferrite catalysts in the degradation of 4-chlorophenol from water under neutral conditions. *Journal of Water Process Engineering* **8**, e37-e49.

Kwnon, B. G., Lee, D. S., Kang, N. & Yoon, J. 1999 Characteristics of p-chlorophenol oxidation by Fenton's reagent. *Water Research* **33**, 2110-2118.

Liu, Y., Jin, W., Zhao, Y., Zhang, G. & Zhang, W. 2017 Enhanced catalytic degradation of methylene blue by α-Fe_2O_3/graphene oxide via heterogeneous photo-Fenton reactions. *Applied Catalysis B* **206**, 642-652.

Lopez, T., Rojas, F., Katz, R., Galindo, F., Balankin, A. & Buljan, A. 2004 Porosity, structural and fractal study of sol–gel TiO_2–CeO_2 mixed oxides. *Journal of Solid State Chemistry* **177**, 1873-1885.

Mamontov, E., Egami, T., Brezny, R., Koranne, M. & Tyagi, S. 2000 Lattice Defects and Oxygen Storage Capacity of Nanocrystalline Ceria and Ceria-Zirconia. *Journal of Physical Chemistry B* **104**, 11110-11116.

Nasralla, N., Yeganeh, M., Astuti, Y., Piticharoenphun, S., Shahtahmasebi, N., Kompany, A., Karimipour, M., Mendis, B. G., Poolton, N. R. J. & Šiller, L. 2013 Structural and spectroscopic study of Fe-doped TiO_2 nanoparticles prepared by sol–gel method. *Scientia Iranica F* **20**, 1018-1022.

Munoz, M., Pedro, Z. M., Casas, J. A., Rodriguez, J. J. 2015 Preparation of magnetite-based catalysts and their application in heterogeneous Fenton oxidation-A review. *Applied Catalysis B* **176-177**, 249-265.

Pouran, S. R., Abdul Raman, A. Z. & Wan Daud, W. M. A. 2014 Review on the application of modified iron oxides as heterogeneous catalysts in Fenton reactions. *Journal of Cleaner Production* **64**, 24-35.

Rivas, F. J., Beltrán, F. J., Frades, J. & Buxeda, P. 2001 Oxidation of p-hydroxybenzoic acid by Fenton's reagent. *Water Research* 35, 387-396.

Shoko, E., Smith, M. F. & McKenzie, R. H. 2009 Mixed valency in cerium oxide crystallographic phases: Valence of different cerium sites by the bond valence method. *Physical Review B* **79**, 134108-134120.

Shukla, P., Wang, S., Sun, H., Ang, H. M. & Tadé, M. 2010 Adsorption and heterogeneous advanced oxidation of phenolic contaminants using Fe loaded mesoporous SBA-15 and H_2O_2. *Chemical Engineering Journal* **164**, 255-260.

Sreeja, PH., & Sosamony, KJ. 2016 A Comparative study of homogeneous and heterogeneous photo-Fenton process for textile wastewater treatment. *Procedia Technol* **24**, 217- 223.

Wang, Y., Shen, X. & Chen, F. 2014 Improving the catalytic activity of CeO_2/H_2O_2 system by sulfation pretreatment of CeO_2. *Journal of Molecular Catalysis A* **381**, 38-45.

Wang, Y., Zhao, H. & Zhao, G. 2015 Iron-copper bimetallic nanoparticles embedded within ordered mesoporous carbon as effective and stable heterogeneous Fenton catalyst for the degradation of organic contaminants, *Applied Catalysis B* **164**, 396-406.

Wei, X., Wu, H. & Sun, F. 2017 Magnetite/Fe-Al-montmorillonite as a Fenton catalyst with efficient degradation of phenol. *Journal of Colloid and Interface Science* **504**, 611-619.

Figures captions

Figure 1 XRD patterns of A: (a) CeTi(1/4), (b) CeTi(1/5), (c) CeTi(1/6), (d) TiO_2, and (e) CeO_2 and B: (a) CeTi(1/5), (b) 3Fe/CeTi–C, (c) 3Fe/CeTi–R, (d) TiO_2, (e) 3Fe/Ti–C, (f) TiO_2, and (g) CeO_2.

Figure 2 H_2-TPR profiles of (a) CeO_2, (b) CeTi(1/5), (c) 3Fe/CeTi–C, (d) 3Fe/CeTi–R, and (e) 3Fe/Ti–C.

Figure 3 TEM images of (a) TiO_2; (b) CeTi(1/5), (c) 3Fe/CeTi–C, and (d) 3Fe/CeTi–R.

Figure 4 XPS spectra of 3Fe/CeTi–C: (a) Fe2p, (b) Ce3d, (c) Ti2p, and (d) O1s.

Figure 5 Evolution of the concentrations of p–HBZ and intermediates over supported Fe catalysts. *H_2O_2/p–HBZ molar ratio=14/1, pH03.2, $m_{catalyst}$=30 mg, T=60 °C.*

Figure 6 Effect of pH on the oxidation of p–HBZ over 3Fe/CeTi–C. *H_2O_2/p–HBZ molar ratio=14/1, $m_{catalyst}$=30 mg, T=60 °C.*

Figure 7 Effect of H_2O_2/p–HBZ molar ratio on the oxidation of p–HBZ over 3Fe/CeTi–C. *$m_{catalyst}$=30 mg, T=60 °C, $pH_0$3.2.*

Figure 8 Plots of $\ln(C_0/C_t)$ *versus* time for the oxidation of p–HBZ over 3Fe/CeTi–C at different temperatures.

Captions for Tables

Table 1 Textural and structural properties of the prepared materials.

Table 2 Initial reaction rates and catalytic properties of supported Fe catalysts for the oxidation of p–HBZ at 60 °C.

Table 3 Catalytic behavior of 3Fe/CeTi–C at different reaction temperatures.